

# Neuroblast Protuberances in the Subventricular Zone of the Regenerative MRL/MpJ Mouse

KASEY L. BAKER,<sup>1,2</sup> STEPHEN B. DANIELS,<sup>2</sup> JESSICA B. LENNINGTON,<sup>1,2</sup>  
THOMAS LARDARO,<sup>1</sup> ALEXANDRA CZAP,<sup>1</sup> RYAN Q. NOTTI,<sup>1</sup> OLIVER COOPER,<sup>3</sup>  
OLE ISACSON,<sup>3</sup> SALVATORE FRASCA JR.,<sup>4</sup> AND JOANNE C. CONOVER<sup>1,2\*</sup>

<sup>1</sup>Center for Regenerative Biology, University of Connecticut, Storrs, Connecticut 06269

<sup>2</sup>Department of Physiology and Neurobiology, University of Connecticut, Storrs, Connecticut 06269

<sup>3</sup>Center for Neuroregenerative Research, McLean Hospital, Harvard Medical School, Belmont, Massachusetts 02478

<sup>4</sup>Department of Pathobiology and Veterinary Science, University of Connecticut, Storrs, Connecticut 06269

## ABSTRACT

The MRL mouse is unique in its capacity for regenerative healing of wounds. This regenerative ability includes complete closure, with little scarring, of wounds to the ear pinna and repair of cardiac muscle, without fibrosis, following cryoinjury. Here, we examine whether neurogenic zones within the MRL brain show enhanced regenerative capacity. The largest neurogenic zone in the adult brain, the subventricular zone (SVZ), lies adjacent to the lateral wall of the lateral ventricle and is responsible for replacement of interneuron populations within the olfactory bulb. Initial gross observation of the anterior forebrain in MRL mice revealed enlarged lateral ventricles; however, little neurodegeneration was detected within the SVZ or surrounding tissues. Instead, increased proliferation within the SVZ was observed, based on incorporation of the thymidine analogue bromodeoxyuridine. Closer examination using electron microscopy revealed that a significant number of SVZ astrocytes interpolated within the ependyma and established contact with the ventricle. In addition, subependymal, protuberant nests of cells, consisting primarily of neuroblasts, were found along the anterior SVZ of MRL mice. Whole mounts of the lateral wall of the lateral ventricle stained for the neuroblast marker doublecortin revealed normal formation of chains of migratory neuroblasts along the entire wall and introduction of enhanced green fluorescent protein-tagged retrovirus into the lateral ventricles confirmed that newly generated neuroblasts were able to track into the olfactory bulb. *J. Comp. Neurol.* 498: 747–761, 2006. © 2006 Wiley-Liss, Inc.

**Indexing terms:** neurogenesis; neural stem cell; neuroblasts; regeneration; migration

Neural stem cells (NSC) support neurogenesis in two major regions of the adult brain, the subgranular layers of the hippocampal dentate gyri and the subventricular zones (SVZ) along the lateral walls of the lateral ventricles (for reviews see Gage, 2000; Alvarez-Buylla et al., 2001; Peterson, 2002; Doetsch, 2003; Imura et al., 2003; Kempermann et al., 2004; Wurmser et al., 2004; Alvarez-Buylla and Lim, 2004). SVZ neurogenesis generates new neurons that migrate as chains along the lateral wall of the lateral ventricle, culminating in the rostral migratory stream (RMS), where chains of neuroblasts transit the anterior forebrain in a restricted pathway and then enter the olfactory bulb (OB). In the OB, SVZ neuroblasts dif-

ferentiate into either granule cell or periglomerular interneurons. To ensure continuous neurogenesis, the unique cytoarchitecture of the SVZ must support stem cell self-renewal, neuronal fate decisions, and tangential chain

Grant sponsor: University of Connecticut Large Grant Fund.

\*Correspondence to: Joanne C. Conover, PhD, Center for Regenerative Biology, University of Connecticut, ATL Building, 1392 Storrs Road, Storrs, CT 06269-4243. E-mail: joanne.conover@uconn.edu

Received 16 May 2005; Revised 19 August 2005; Accepted 9 May 2006

DOI 10.1002/cne.21090

Published online in Wiley InterScience (www.interscience.wiley.com).

migration. Studies have shown that interventions effecting normal regulatory signaling mechanisms within the SVZ can act either to diminish or to enhance neurogenesis. For example, infusion of epidermal growth factor (EGF) into the lateral ventricles diminishes neurogenesis and supports gliogenesis (Doetsch et al., 2002). Also, introduction of truncated, tyrosine kinase-deficient EphB2 into the lateral ventricles expands glial populations within the SVZ, although the mechanism for this expansion is not fully understood (Conover et al., 2000). Conversely, transforming growth factor- $\alpha$  (TGF $\alpha$ ; Cooper and Isacson, 2004) and the bone morphogenic protein (BMP) antagonist noggin promote SVZ neurogenesis (Lim et al., 2000), whereas the cytokines leukemia inhibitory factor (LIF) and ciliary neurotrophic factor (CNTF) act through their gp130 receptor complex to promote NSC renewal (Shimazaki et al., 2001; Chojnacki et al., 2003). Although these short-term perturbations of SVZ signaling molecules result in dramatic alterations to SVZ cytoarchitecture, it is unclear how the SVZ would compensate for and support long-term, sustained increases in neurogenesis.

The MRL/MpJ mouse (referred to here as MRL) is an inbred strain, with a composite genetic background from four different strains of mice: LG (75%), AKR (12.6%), C3H (12.1%), and C57BL/6 (0.3%; The Jackson Laboratory, Mouse Genome Informatics). Unique to the MRL mouse is its potential for regenerative wound healing (Lefterovich et al., 2001). After tissue removal by hole punch to the ear pinnae, MRL mice regenerate ear tissue with little scarring and complete restoration of tissue architecture (Clark et al., 1998). In addition, cryoinjury to the heart of MRL mice results in replacement of wounded tissue without fibrosis (Lefterovich et al., 2001). These phenomena appear to be heightened responses to wound healing, more reminiscent of regeneration seen in primitive vertebrates than the limited repair mechanisms found in tissues of most mammals. Is there something unique about MRL stem cell niches and their capacity for regeneration?

To address this possibility, we examined the largest neurogenic region in the adult brain, the SVZ, in MRL mice. Previous, electron microscopic investigations of the SVZ have revealed the major cell types and cell-cell contacts along the lateral wall of the lateral ventricles (Doetsch et al., 1997, 1999; Conover et al., 2000). In comparison with the outbred strain, CD-1, we found increased proliferation and alterations in SVZ cytoarchitecture in MRL mice. Along the anterior SVZ, nests of neuroblasts bulged into the lateral ventricle. Whereas an intact ependymal monolayer was maintained adjacent to the protuberance, in other regions of the SVZ discontinuities in the ependyma were seen where astrocytic processes contacted the ventricle space.

## MATERIALS AND METHODS

### Animals

MRL/MpJ (abbreviated here as *MRL*), LG, and C57BL/6J mice were obtained from The Jackson Laboratory. CD-1 mice were purchased from Charles River. All strains of mice were analyzed at 2 months of age. Animal procedures were performed under protocols approved by the Institutional Animal Care and Use Committee of the University of Connecticut and conformed to National Institutes of Health guidelines.

### Immunocytochemistry

Male mice were perfused transcardially with 0.9% saline followed by 3% paraformaldehyde in phosphate-buffered saline (PBS; pH 7.4). Brains were removed and postfixed overnight in 3% paraformaldehyde at 4°C. Brains were washed in PBS three times for 10 minutes each, prior to cutting 50- $\mu$ m sections with a vibratome (VT-1000S; Leica, Wetzlar, Germany). Free-floating sections were washed in 0.1% Triton X-100 (Sigma, St. Louis, MO) in PBS three times for 10 minutes each, blocked in 10% goat serum (Sigma) in PBS/0.1% Triton X-100 for 1 hour, and incubated with primary antibody. The source, characterization, and controls are listed below for each antibody used. Antibromodeoxyuridine (BrdU; catalog No. OBT0030; Accurate Chemical and Scientific Corporation, Westbury, NY) was raised in rat and reacts with BrdU in single-stranded DNA or BrdU attached to protein carrier or free BrdU (manufacturer's technical information). The monoclonal anti-BrdU IgG2a antiserum was used at 5  $\mu$ g/ml. No staining was seen in cases in which animals were not infused with BrdU. Anticaspase-3 (catalog No. AF835, lot CFZ32; R&D Systems, Minneapolis, MN) was raised in rabbit against KLH coupled synthetic peptide CRGTELDGCIETD corresponding to amino acids 163–175 of human caspase-3. On Western blots, the antibody detected the p17 subunit of caspase-3 and not the precursor form (manufacturer's technical information and Paitel et al., 2003), and it was shown that this caspase-3 antiserum labels only apoptotic cells in the brain (Kuo et al., 2005). We used affinity-purified, polyclonal IgG caspase-3 antiserum at 0.3  $\mu$ g/ml. Antidoublecortin (DCX; catalog No. SC-8066; Santa Cruz Biotechnology, Santa Cruz, CA) was raised in goat against an epitope of human doublecortin isoform a. This epitope is blocked by a peptide corresponding to residues 422–437 of human DCX (accession No. NP 00054 of the NCBI database), and staining is abolished. Western blot analysis of fresh brain hippocampi revealed a single band at 50 kDa (Mizuguchi et al., 1999; Jin et al., 2004). Affinity-purified, polyclonal IgG antiserum was used at a concentration of 1  $\mu$ g/ml and stained cells with the morphology and cell distribution of neuroblasts, as previously reported (Gleeson et al., 1999; Jin et al., 2004). Antiglial fibrillary acidic protein (GFAP; catalog No. Z0334, lot 096; Dako, Carpinteria, CA) was raised in rabbit against cow GFAP isolated from spinal cord. A single polypeptide band was detected by Western blot at 50–53 kDa (Toma et al., 2001). We used the polyclonal anti-GFAP IgG antiserum at 4.1  $\mu$ g/ml and obtained staining patterns identical to those described in previous reports of astrocyte cellular morphology and distribution in the brain (Sawant et al., 1994). Anti-Ki67 (catalog No. NCL-Ki67p; Novocastra, Newcastle upon Tyne, United Kingdom) was raised in rabbit against a prokaryotic recombinant fusion protein corresponding to a 1,086-bp Ki67 motif of the cDNA fragment (manufacturer's technical information), and a double band at 345–395 kDa was detected by Western blot analysis (Key et al., 1993). The polyclonal anti-Ki67 antibody was used at 24 ng/ml. After a 2-hour pulse with BrdU, all BrdU<sup>+</sup> cells also stained with Ki67 antiserum. The doubly positive BrdU<sup>+</sup>, Ki67<sup>+</sup> population was a subpopulation of the total Ki67<sup>+</sup> population. In addition, as a positive control, the polyclonal Ki67 antiserum was found to stain newborn cells that express cell cycle proteins in brain and tumor tissue (Quinones-

Hinojosa et al., 2006). Anti-PECAM-1 (also known as anti-CD31; catalog No. 553370; BD Biosciences/PharMingen, San Diego, CA) was raised in rat against 129/Sv mouse-derived endothelioma cell line tEnd.1. The monoclonal IgG2a antiserum was purified by affinity chromatography and recognizes only the 130-kDa CD31 protein by Western blot analysis (manufacturer's technical information). Antiserum to PECAM-1 was used at 1.7  $\mu\text{g}/\text{ml}$ . Staining with this antiserum was identical to that described in previous reports showing blood vessels in the adult mouse brain (van Praag et al., 2005). Antipolysialylated neural cell adhesion molecule (PSA-NCAM; catalog No. AbC0019; AbCys, Paris, France) was raised in mouse against alpha 2-8 linked neuraminic acid ( $n > 10$ ). By using hippocampal brain tissue, a 180-kDa band was recognized by Western blotting (Bouzioukh et al., 2001; Jin et al., 2004). We used the monoclonal PSA-NCAM IgM antiserum at 0.125  $\mu\text{g}/\text{ml}$  and detected staining in cells with the morphology and distribution of neuroblasts in the SVZ similar to that in previous studies (Rousselot et al., 1995). Sections were incubated with appropriate Alexa Fluor dye-conjugated secondary antibodies (Molecular Probes, Eugene, OR) for 1 hour, washed three times for 10 minutes each in PBS (pH 7.4), and then incubated for 5 minutes in 2  $\mu\text{g}/\text{ml}$  Hoechst 33342 (Sigma). All tissue analyzed showed no labeling when the primary antibody was omitted and the secondary antibody alone was used as a control. Sections were washed for 5 minutes in PBS and coverslipped using Aquapolymount (Polysciences, Warrington, PA).

### BrdU immunocytochemistry

Mice were injected with 300 mg BrdU/kg 2 hours prior to perfusion (2-hour pulse; Cameron and McKay, 2001). BrdU immunostaining of 50- $\mu\text{m}$  sections was conducted as described previously (Lie et al., 2002). Epifluorescence imaging of BrdU<sup>+</sup> and Ki67<sup>+</sup> cells along the lateral wall of the lateral ventricle was performed with a Zeiss Axioskop 2+ microscope (Carl Zeiss MicroImaging, Inc., Thornwood, NY) and Retiga 1300 EX digital camera (Q-Imaging, Burnaby, British Columbia, Canada). BrdU<sup>+</sup> and Ki67<sup>+</sup> cells along the lateral wall of the lateral ventricle were counted in Openlab 3.1.5 imaging software (Improvision, Lexington, MA) in 18 anterior forebrain sections (50  $\mu\text{m}$ ), from coordinates 0.5–1.4 anterior, relative to bregma. This region contains the protuberances found in MRL mice. At least three mice were used for each group, and statistical analyses were performed via Student's *t*-test. BrdU/DCX and BrdU/GFAP colabeling was imaged with a Leica TCS SP2 confocal system together with a Leica DMIRE2 microscope and Leica confocal software (version 2.61).

### Cell death

After anticaspase-3 immunostaining, caspase-3-positive cells within the SVZ were counted in 22 sections (50  $\mu\text{m}$ ) from coordinates 0.5–1.4 anterior/posterior, relative to bregma, as described above. For cell counts in the RMS and OB, caspase<sup>+</sup> cells were counted in every section (50  $\mu\text{m}$ ) within the entire region of both structures. At least three mice were used for each group, and statistical analyses were performed via Student's *t*-test.

### Whole mounts

Whole mounts of the entire lateral wall of the lateral ventricle were prepared as previously described (Doetsch and Alvarez-Buylla, 1996) and immunostained for DCX

(Santa Cruz Biotechnology). Whole mounts were placed onto glass slides, coverslipped with Aquapolymount (Polysciences), and imaged by epifluorescence microscopy.

### Brain histology

Mice were perfused and brains postfixed as described above. To visualize Nissl substance, we followed standard protocols. Briefly, anterior forebrain coronal sections are placed onto Superfrost Plus slides and dried overnight. Tissue was then taken through a series of ethanol (70%, 50%, 25%; 2 minutes each) and placed in 0.5% cresyl violet solution for 2 minutes. Slides were then dehydrated in 25%, 50%, and 75% ethanol and placed in a differentiator (acetic acid in 95% ethanol, 1:125) for 1.5 minutes. Dehydration steps continued with 95% and 100% ethanol, twice each for 2 minutes, followed by three rinses in xylene for 2 minutes each. Slides were mounted with DPX and coverslipped. Coronal sections were imaged on a Zeiss Imager Z1 microscope with an AxioCam MRm camera and Axio-Vision 4.5 software (Zeiss). Brain tissue was routinely processed for paraffin embedding, and coronal slices (6  $\mu\text{m}$ ) were cut, mounted onto slides, dried overnight, stained with hematoxylin and eosin, and coverslipped with DPX mountant.

### Lateral ventricle volume, striatal volume, and RMS diameter measurements

Striatal and lateral ventricle volumes of CD-1 and MRL mice were calculated from cresyl violet-stained sections with a brightfield microscope (Zeiss Axioskop 2+) and a stereology workstation (MicroBrightField, Williston, VT). The Cavalieri estimator was implemented on one-third of the 40- $\mu\text{m}$  sections between +1.70 mm and -0.10 mm for the striatum and between +1.54 mm and -0.10 mm for the lateral ventricles, relative to Bregma. The coefficient of error was used to evaluate the precision of the calculated volumes ( $P < 0.05$ ).

To determine RMS diameters, 50- $\mu\text{m}$  coronal sections (vibratome) of fixed brain were labeled for PSA-NCAM and GFAP. Fluorescent images were captured (Axioskop 2+, Zeiss; and Retiga EX, Q-Imaging System, Burnaby, Canada) of the RMS. Measurements of the area of the RMS were performed in Openlab 3.1.5 (Improvision, Lexington, MA). Three RMS measurements were taken at 3.67, 3.72, and 3.77 mm distal to the beginning of the olfactory bulbs, and mean values  $\pm$  SEM were calculated. At least three mice were used for each group, and statistical analyses were performed via Student's *t*-test.

### Electron microscopy

Male mice were perfused transcardially with 0.9% saline, followed by 2% paraformaldehyde/2.5% glutaraldehyde in 0.1 M PB (pH 7.4). Heads were postfixed by immersion overnight in 2% paraformaldehyde/2.5% glutaraldehyde in 0.1 M PB; brains were removed and washed in PB three times for 40 minutes each. Three 300- $\mu\text{m}$  sections of the anterior forebrain were cut with a vibratome, pinned to plastic dishes to prevent buckling, and processed as described previously (Conover et al., 2000). Briefly, sections were postfixed with 2% OsO<sub>4</sub> in 0.1 M PB for 1.25 hours, unpinned, and dehydrated through a graded EtOH series. Sections were en bloc stained in 2% uranyl acetate at the 70% EtOH step for 1.5 hours. After dehydration, whole sections were twice washed in pro-

pylene oxide and embedded in a SPI-PON 812 (SPI Supplies, Westchester, PA)/Araldite 506 (Ernest F. Fullam, Inc., Latham, NY) mixture between aclar sheets. After polymerization, the SVZ regions were cut from each section and reembedded in the same epoxy mixture in capped inverted Beem capsules. Thin sections were cut with a diamond knife, placed onto Formvar-coated slot grids, and heavy-metal-stained with uranyl acetate and lead citrate. Electron micrographs were digitized with an Epson 1680 scanner (1,600 dpi), and montages were constructed of the SVZ in Adobe Photoshop. A gradient tool was used to adjust the brightness of the images to match the intensity in adjacent images. Cell types were identified based on previously described criteria (Doetsch et al., 1997; see also Fig. 4).

### Retrovirus injections and analysis

High-titer ( $2\text{--}5 \times 10^8$  cfu/ml) replication-incompetent retrovirus encoding enhanced green fluorescent protein (eGFP; a kind gift from Dr. Joseph LoTurco, University of Connecticut, Storrs, CT), was synthesized as previously described (Belluzzi et al., 2003). Two-month-old MRL or CD-1 mice were anesthetized with isoflurane and placed in a stereotaxic apparatus, and the anterior lateral ventricle was unilaterally injected, using the stereotaxic coordinates of 0.5 mm anterior/posterior, 1.2 mm lateral, and 2.2 mm ventral relative to bregma, with a 0.5- $\mu$ l solution of eGFP retrovirus. Twenty-four hours, 2 weeks, or 4 weeks postinjection, mice were transcardially perfused and the brains fixed overnight in 3% paraformaldehyde. Fifty-micrometer horizontal serial sections were cut with a vibratome and eGFP<sup>+</sup> cells imaged by confocal microscopy.

## RESULTS

NSCs are located in the adult mammalian SVZ (Reynolds and Weiss, 1992; Luskin, 1993; Morshead et al., 1994; Doetsch et al., 1999), which lies adjacent to the lateral walls of the lateral ventricles. New neurons, produced from NSCs, migrate to the olfactory bulb, where it is thought that they replace older neurons involved in regulating incoming activity from the olfactory epithelium (Gheusi et al., 2000; Cecchi et al., 2001; Petreanu and Alvarez-Buylla, 2002). To determine whether this regenerative zone is enhanced in MRL mice, we initially examined the neurogenic SVZ in anterior forebrain sections of 2-month-old mice. It was immediately apparent that MRL mice have enlarged lateral ventricles compared with control CD-1 or C57BL/6 mice (Fig. 1a–c). Particularly conspicuous was the open ventral portion of the lateral ventricle, which typically exhibits a tight apposition of the two ependymal surfaces (Fig. 1b–c, CD-1 and C57BL/6 brackets; Paxinos, 2001). Volume measurements of the lateral ventricles showed a threefold increase in MRL compared with CD-1 mice (Fig. 1d), reflecting, in part, the open ventral aspect of the lateral ventricle. Alterations to other brain structures were not observed, and volume measurements of the neighboring striatum showed no significant difference between MRL and CD-1 mice (Fig. 1e). For CD-1 mice, we calculated that lateral ventricle volume as 0.11% of total brain volume (based on brain volumes listed at [www.mbl.org](http://www.mbl.org) and [www.nervenet.org](http://www.nervenet.org)). Therefore, based on these calculations, a threefold increase in lateral ventricle volume in MRL mice would result in either small

cumulative decreases in other brain structures to maintain brain size or an incrementally small increase in total brain size. Fresh brain volume measurements showed a small but significant difference between MRL and CD-1 mice (Fig. 1g), enough, however, to account for some of the lateral ventricle increase seen in MRL mice.

### Increased proliferation with little cell death found in SVZ of MRL mice

Does decreased NSC proliferative capacity or increased neurodegeneration contribute to the enlarged ventricles? To examine proliferation in the SVZ of MRL mice, we quantified the fraction of SVZ cells in S phase by counting the number of BrdU<sup>+</sup> cells relative to the number of cells positive for the general proliferation marker Ki67 along the lateral wall of the lateral ventricle of 2-month-old CD-1 and MRL mice. Ki67 labels cells in G1, S, G2, and mitosis (Scholzen and Gerdes, 2000). Mice were injected with 300 mg BrdU/kg (Cameron and McKay, 2001) and perfused 2 hours postinjection (2-hour pulse). Anterior forebrain coronal sections (50  $\mu$ m) were immunostained for BrdU (Fig. 2a,b) and Ki67, and positive cells were counted along the lateral wall of the lateral ventricle, from coordinates 0.5–1.42 anterior relative to bregma (Fig. 2c; Paxinos, 2001). The ratio of BrdU<sup>+</sup> cells/total Ki67<sup>+</sup> cells provided a labeling index for cell cycle length within the SVZ, allowing BrdU-incorporating cells to be evaluated based on total number of cycling cells within this specific region. In mammalian cells, the length of S phase remains relatively constant, whereas the length of G1 regulates the rate of proliferation (DiSalvo et al., 1995; Chenn and Walsh, 2002). Within the defined coordinates that encompassed the anterior SVZ (see schematic in Fig. 1), we detected an increase in BrdU<sup>+</sup> cells in the SVZ of MRL compared with CD-1 mice (Fig. 2a–c). However, no significant difference in the ratio of BrdU<sup>+</sup> cells/total Ki67<sup>+</sup> cells was detected between the two strains (Fig. 2d), indicating that MRL progenitor cells do not divide significantly faster than CD-1 progenitors. Instead, it appears that the total progenitor pool is larger in MRL mice.

Programmed cell death has been implicated in regulating the progenitor pool in the proliferative ventricular zones during development (Thomaidou et al., 1997; Roth et al., 2000; Putz et al., 2005). To determine the level of cell death along the SVZ and RMS and within the OB, we examined active caspase-3 staining associated with these structures. Caspase-3 is a key enzyme (Blaschke et al., 1996, 1998; Thomaidou et al., 1997; Pompeiano et al., 2000). We detected similar levels of caspase-3<sup>+</sup> cells along the SVZ (Fig. 2e) and RMS (Fig. 2f) of both MRL and CD-1 mice. In support of these findings, electron micrographs of the SVZ showed very few necrotic cells along the lateral ventricle wall of MRL mice (see Fig. 5a,b). However, active caspase-3 staining was significantly greater in the OB of MRL mice (Fig. 2g).

### Nests of neuroblasts within the SVZ wall

How does the SVZ of MRL mice accommodate excess cell proliferation? Histological examination revealed focal, protuberant, subependymal aggregates or nests of cells along the lateral ventricle wall of 2-month-old MRL mice (Fig. 3a). These abnormally large nests occurred in the anterior portion of the SVZ (see schematic in Fig. 1), corresponding to regions of increased cell proliferation, and were not found in the SVZ of CD-1 or C57BL/6 mice.

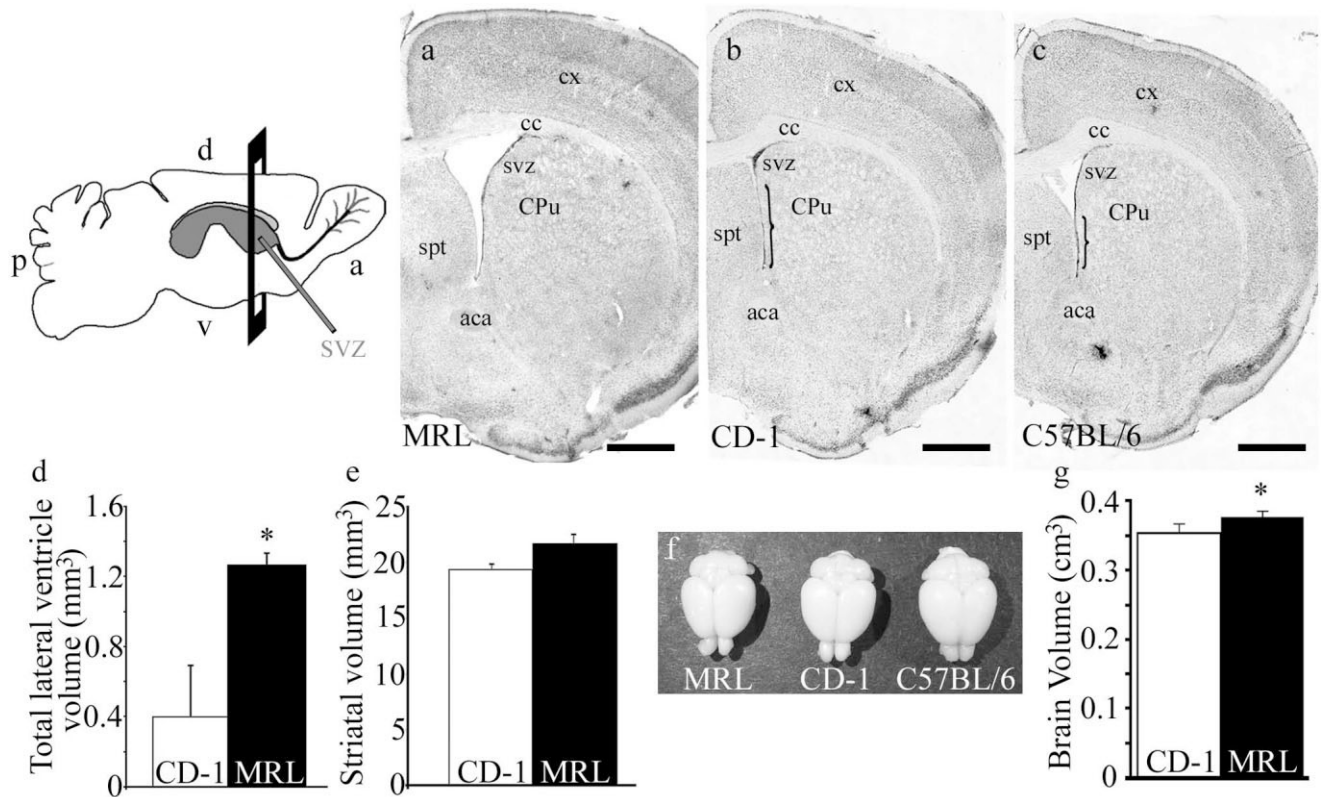


Fig. 1. MRL mice have enlarged lateral ventricles. Nissl-stained coronal sections through the anterior forebrain at the level of the anterior lateral ventricle (indicated in schematic by vertical plane bisecting sagittal view of brain) show enlarged ventricle of MRL mice (a) compared with CD-1 (b) and C57BL/6 (c) mice. Brackets indicate lateral-medial wall apposition in CD-1 and C57BL/6 brains. cx, Neocortex; cc, corpus callosum; SVZ, subventricular zone; CPu, caudate putamen; spt, septum; ac, anterior commissure (anterior). **d**: Volume

measurements of the lateral ventricle of MRL mice show a significant threefold increase compared with CD-1 mice. However, the volumes of the neighboring striatum (caudate putamen) of CD-1 and MRL mice were not significantly different (e; two-tailed *t*-test,  $*P < 0.05$ ). **f**: Overt differences in brain size are not discernible; however, measurements of brain volumes indicate a small but significant increase in MRL vs. CD-1 (g; two-tailed *t*-test,  $*P < 0.05$ ). Scale bars = 1 mm.

However, the MRL component strain LG (contributes 75% of MRL genomic background) exhibited similar protuberant subependymal nests along the margin with the ventricle (Fig. 3b).

Detailed examination of the cytoarchitectural organization of the SVZ of MRL mice was performed by transmission electron microscopy (EM). Ultrathin, coronal sections were imaged, and contiguous EM micrographs were assembled into a montage to show the entire lateral wall of the lateral ventricle. Montages were then colorized based on cell morphological criteria, as previously reported (Doetsch et al., 1997; Garcia-Verdugo et al., 1998; Conover et al., 2000; see Fig. 4). Because of the extended length of the lateral ventricle, the dorsal (D) and ventral (V) portion of the MRL lateral ventricle is shown in Figure 5a and b, respectively, whereas the entire D/V aspect of the CD-1 ventricle is shown in Figure 5c. EM-based reconstructions of the MRL SVZ revealed, in the ventral zone of the anterior SVZ, an accumulation of numerous neuroblasts into foci or neuroblastic nests (compare Fig. 5b and c). These protuberant nests of cells were composed primarily of neuroblasts (red cells), and the large aggregates of neuroblasts were, in turn, margined by astrocytes (green cells), similar to the cytoarchitectural arrangement

previously described for CD-1 mice, in which astrocytes ensheath chains of migrating neuroblasts (Lois et al., 1996; Doetsch et al., 1997). In addition, we detected an increase in the number of astrocytic processes (green cells, arrows) positioned within the ependymal monolayer (yellow cells) and contacting the ventricular lumen (Fig. 5a,b vs. c).

To confirm the composition of these SVZ nests of cells and to determine whether increased cell proliferation contributed to neurogenesis, we immunostained 50- $\mu$ m vibratome sections for DCX (a marker of neuroblasts), GFAP (a marker of astrocytes), and BrdU (cells in S phase of the cell cycle). Epifluorescence microscopy verified that DCX<sup>+</sup> cells made up the nests in MRL protuberances and that these neuroblastic nests were surrounded by SVZ astrocytes (Fig. 6a). In addition, several DCX<sup>+</sup> cells found within protuberances took up BrdU following a 2-hour pulse (Fig. 6b,c), indicating that the protuberant nests contained actively dividing neural progenitor cells.

#### Protuberant nests and their association with blood vessels

Previous studies have shown NSCs concentrated around blood vessels (Palmer et al., 2000; Capela and

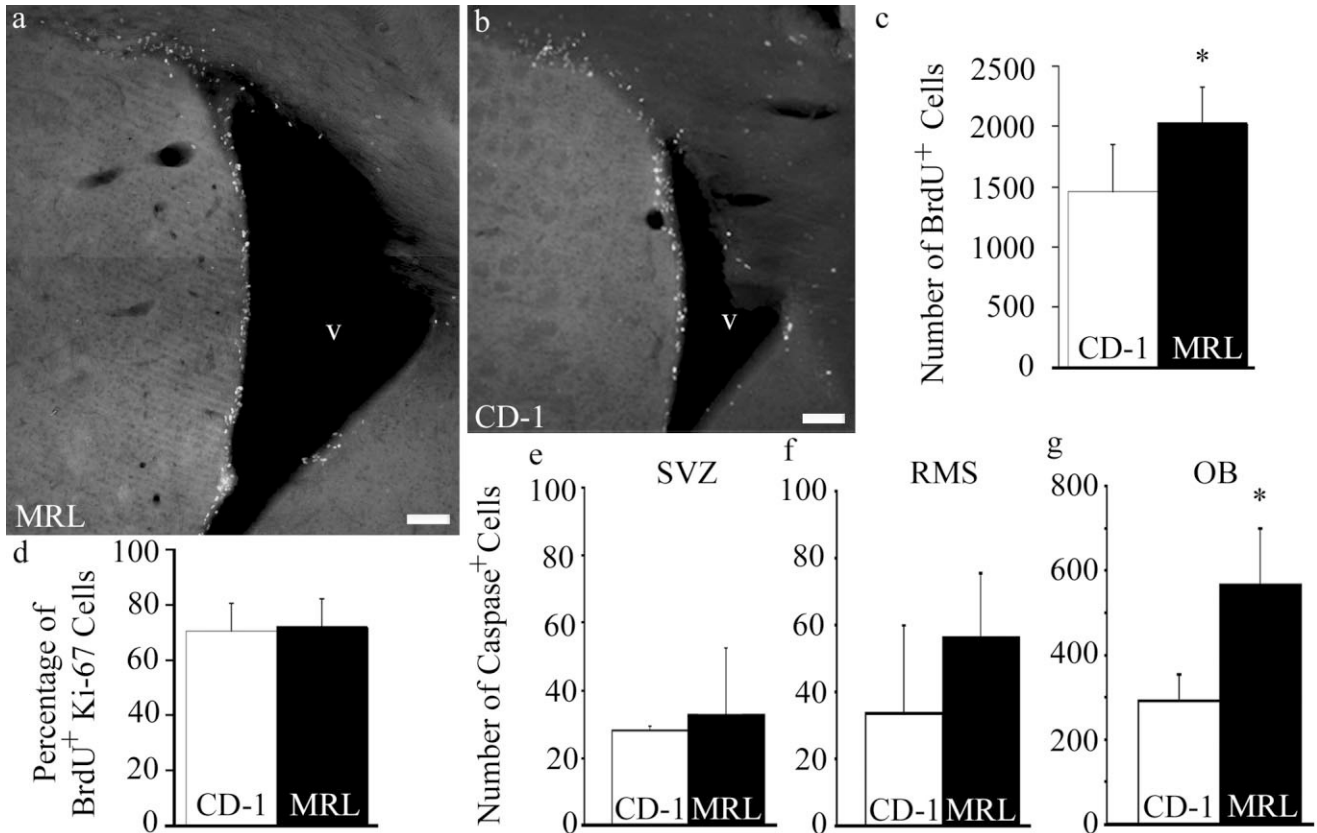


Fig. 2. The SVZ progenitor pool is increased in MRL mice. **a,b:** After a 2-hour pulse, BrdU<sup>+</sup> cells (white dots) are shown along the lateral wall of the lateral ventricle in MRL and CD-1 mice. (Note the increased size of the lateral ventricle wall in MRL.) **c:** Counts of BrdU<sup>+</sup> cell along the lateral wall of the lateral ventricle show a significant increase in MRL vs. CD-1 mice (two-tailed *t*-test, \**P* < 0.08). However, the percentage of progenitor cells (Ki67<sup>+</sup> cells) labeled

with BrdU after a 2-hour pulse is not different in MRL and CD-1 mice (**d**), indicating that a larger progenitor pool exists in MRL mice. **e,f:** Similar levels of caspase-3<sup>+</sup> cells were detected in the SVZ and RMS of MRL and CD-1 mice. **g:** A twofold increase in caspase<sup>+</sup> cells is found in the OB of MRL vs. CD-1 mice (\**P* < 0.05 by two-tailed *t*-test). Scale bars = 100  $\mu$ m.

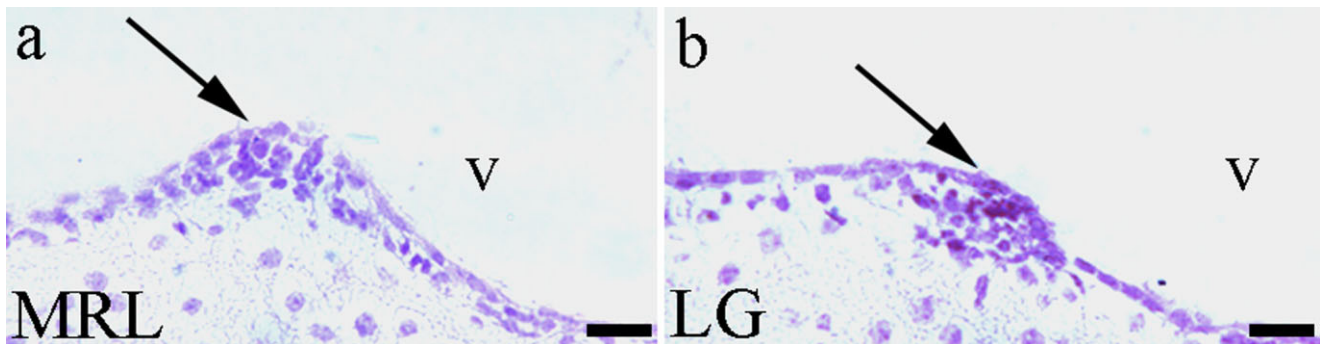
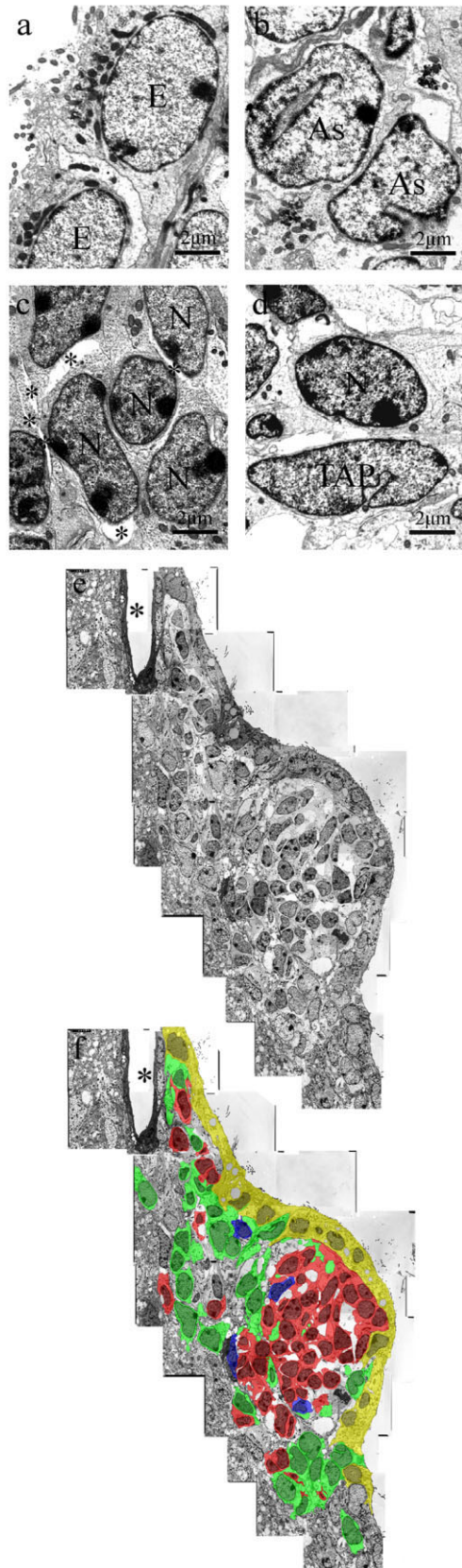


Fig. 3. Protuberant subependymal nests are also found in LG mice, an MRL component strain. Hematoxylin- and eosin-stained coronal sections of the lateral wall of the lateral ventricle show similar protuberances in MRL (**a**) and LG (**b**) mice (arrows). Scale bars = 25  $\mu$ m.

Temple, 2002), thus allowing direct contact between the stem cell and the endothelial cells of blood vessels. In culture, it has been shown that NSCs in close proximity to endothelial cells increase their rate of proliferation and maintain their undifferentiated state (Shen et al., 2004). EM analysis revealed blood vessels located along the pe-

riphery of the entire SVZ, close to the boundary with the striatum in both CD-1 and MRL mice and often associated with nests of neuroblasts (see Figs. 4e, 5a–c). Here, we note the proximity of capillaries to SVZ protuberances. Particularly striking is the example shown in Figure 7, where a blood vessel is found in the center of a neuroblas-



tic protuberance. A series of semithin, toluidine blue-stained sections spanning 60  $\mu\text{m}$  reveals the close association between this blood vessel and the protuberance (Fig. 7b). The cellular organization around blood vessels, whether next to or within protuberances, is similar to that also found throughout the SVZ in control CD-1 mice. In all cases, astrocytes are in direct contact with the basal lamina of either the pericytes or the endothelial cells (Fig. 7d,e) that encircle the blood vessel. Neuroblasts (red cells) or the occasional TAP cell (blue cells) then surround these astrocytes. Confocal images demonstrating the close association between blood vessels with neuroblasts of the SVZ are shown in Figure 7f,g. Although the connection between neurogenic regions and blood vessels is already known (Palmer et al., 2000; Capela and Temple, 2002), our results further illustrate the importance of this connection.

### Does the MRL SVZ support neuroblast migration?

The neuroblast protuberances detected along the SVZ of MRL mice are somewhat reminiscent of heterotopias found during aberrant embryonic development (Brunstrom et al., 1997; Gleeson et al., 1998; Fox et al., 1998; des Portes et al., 1998; Tullio et al., 2001). Heterotopias are commonly a result of migration defects that result in newly generated neurons locating to ectopic sites. To determine whether the accumulation of neuroblasts seen in the SVZ of MRL mice was the result of a neuroblast migration defect, we examined whole mounts of the lateral wall of the lateral ventricles stained for DCX (Gleeson et al., 1998). We observed an abundance of chains of migrating neuroblasts along the entire lateral wall of the lateral ventricle in MRL mice (Fig. 8a), similar to the chains found in control CD-1 mice (Fig. 8b), suggesting that SVZ-generated neuroblasts incorporate into migratory chains.

Newly generated neuroblasts from the SVZ enter the RMS for their final migration into the OB. To investigate whether alterations occur in the RMS of MRL mice, we measured the diameter of the RMS at three levels in corresponding sections of 2-month-old MRL and CD-1 mice. Significantly increased RMS diameters were detected in MRL mice (Fig. 8c). To examine migration of SVZ neuroblasts through the RMS and into the OB, we injected eGFP-tagged retrovirus into the lateral ventricle (24 hours postinjection; Fig. 8f–h) and tracked labeled SVZ progenitor cells into the OB at 2 and 4 weeks. By 4 weeks postinjection, SVZ-generated neuroblasts from MRL mice had entered the OB and migrated to the correct regions of the OB (periglomerular layer, shown in Fig. 8f). However, we could still detect eGFP-labeled neuroblasts in the RMS

Fig. 4. Characteristics and coding of SVZ cell types, based on Doetsch et al. (1997). **a:** Ependymal cells (E): spherical nuclei, many mitochondria, lipid droplets (not shown), cilia. **b:** Astrocytes (As): irregular nuclei, frequently invaginated, intermediate filaments (not observable at magnification presented here), many mitochondria. **c:** Neuroblasts (N): elongated, clustered with spaces between cells (asterisk), microtubules (not observable at this magnification). **d:** TAP (transit amplifying): large, irregular nuclei with deep invaginations, many mitochondria. **e,f:** EM micrograph of MRL protuberance before and after color-coding of SVZ cell types. Scale bars = 2  $\mu\text{m}$  in a–d; 20  $\mu\text{m}$  in f (applies to e,f).

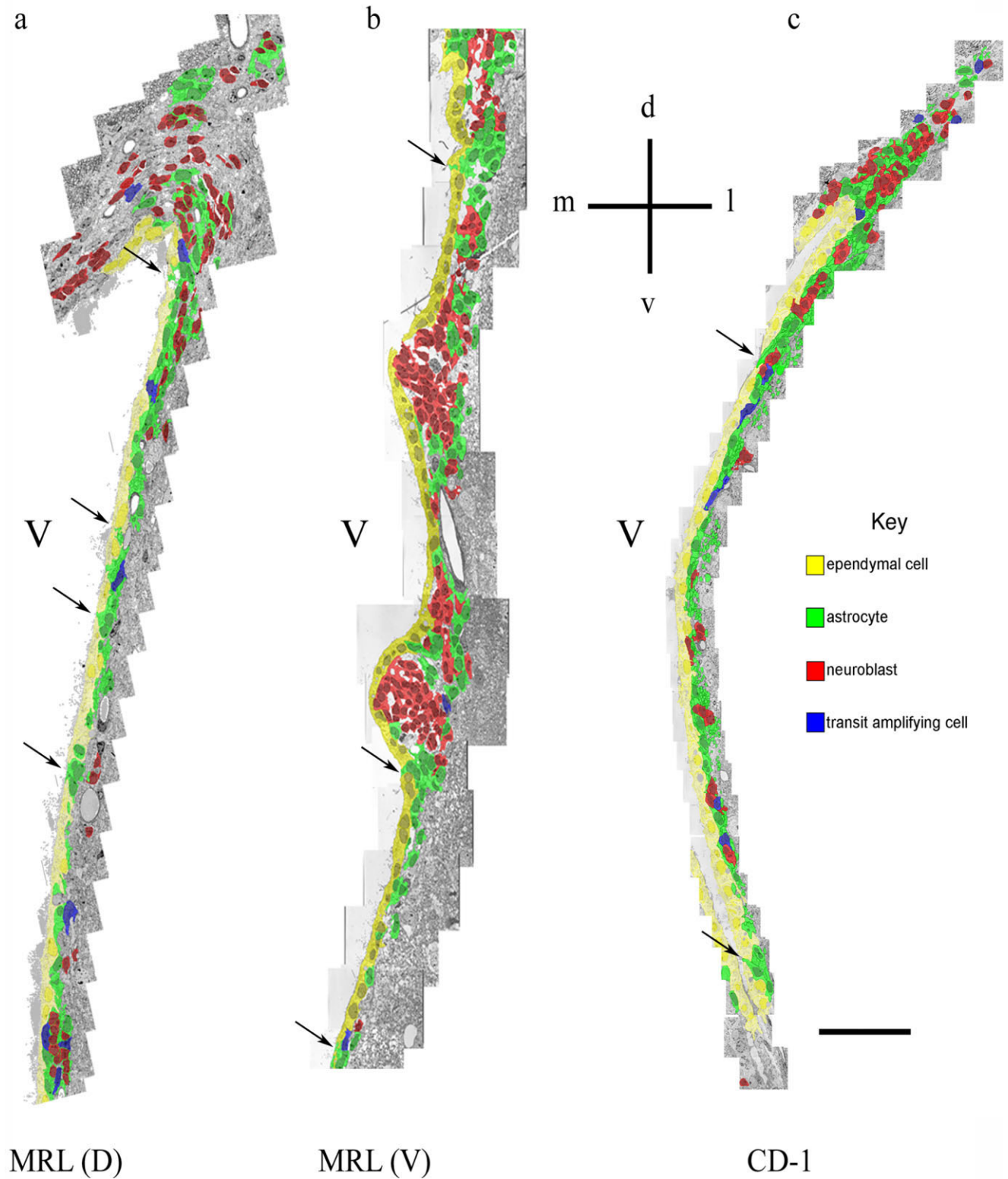


Fig. 5. Transmission electron microscopy (EM) analysis of the anterior SVZ of MRL mice reveals unique cytoarchitectural organization. Color-coded reconstructions of the dorsal (a) and ventral (b) coronal aspects of the anterior lateral wall of the lateral ventricle of an MRL mouse were assembled. Protuberant nests are found along the ventral wall and are separated from the ventricle lumen by an intact

ependyma. However, numerous SVZ astrocytic processes interpose within the ependyma of MRL mice at other regions (a,b, arrows), whereas few interpolated astrocytes are found along the ventricle of CD-1 mice (c, arrows). Orientations of dorsal/ventral and medial/lateral are shown. V, ventricle. Scale bar = 50  $\mu$ m.

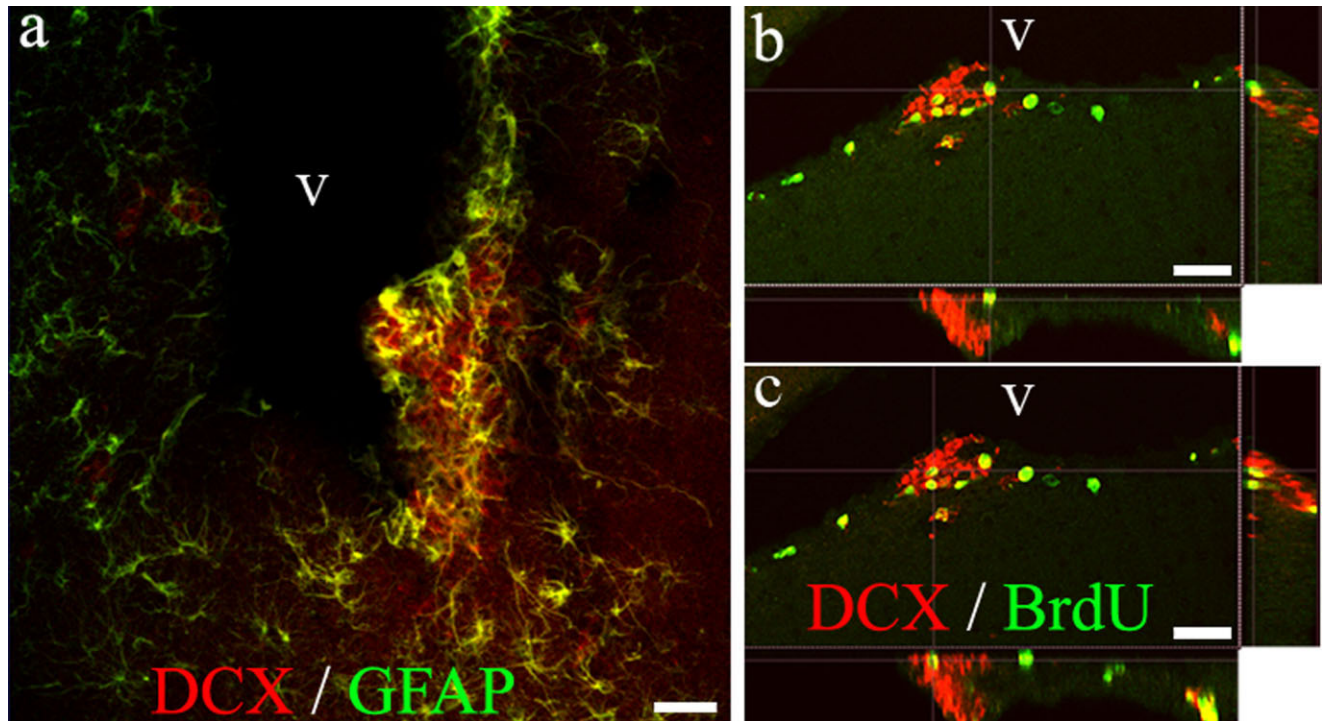


Fig. 6. Protuberant subependymal nests contain dividing neuroblasts. **a:** The protuberances are made up primarily of neuroblasts [doublecortin (DCX)-positive cells] and surrounding astrocytes [glial fibrillary acidic protein (GFAP)-positive cells]. Yellow cells represent bleed-through; no colocalization of DCX<sup>+</sup> and GFAP<sup>+</sup> is detected in protuberances. **b,c:** After a 2-hour pulse, several neuroblasts (DCX<sup>+</sup>)

within the protuberance incorporate the thymidine analogue BrdU, indicating the presence of actively dividing neuroblasts in the protuberant nests. Colocalization of DCX and BrdU in two different cells within a protuberance is shown. Orthogonal views indicate one unique nucleus. Scale bars = 25  $\mu$ m.

4 weeks postinjection in MRL mice (Fig. 8h) but not in CD-1 mice.

## DISCUSSION

The SVZ is the largest neurogenic zone in the adult mammalian brain. In rodents, newly generated SVZ neurons continuously replace granule and periglomerular interneuron populations within the OB. However, it is not clear what regulates supply and demand for neurogenesis within the SVZ. Here, we report that the “regenerative mouse” MRL/MpJ (MRL) displays heightened proliferation along the lateral ventricles, with an accumulation of neuroblasts into large subependymal nests. In addition, at other locations along the lateral ventricle wall, increased numbers of astrocytes interpolate within the ependyma and contact the ventricle. However, despite these alterations, some basic organizational components of the SVZ niche are maintained in MRL mice. For example, aggregates of neuroblasts are still organized into chains, and these chains are surrounded by astrocytes, thus maintaining the characteristic features of SVZ neuroblast chain migration. In addition, cell composition around protuberant neuroblastic nests includes the occasional transit-amplifying progenitor (TAP) cell, close association with astrocytes, and the proximity of endothelial cells of blood vessels, all features common to the cytoarchitectural organization found in control animals. Therefore, it appears that the neurogenic SVZ found in MRL mice maintains

key niche components that can effectively support neurogenesis.

### Vascularization of SVZ protuberances

The dynamic cross-talk between neurons and blood vessels is critical in the development of both the nervous system and the vasculature (for review and references see Weinstein, 2005). Several studies demonstrate that ligands used for axonal guidance in the nervous system are also necessary for the design of vascular architecture. Some of the best studied examples include the bidirectional signaling of the Ephs/ephrins, the secreted netrins and their associated receptors, and vascular endothelial growth factor (VEGF). The duality of effects seen with these and other signaling molecules has led to the proposal that cues act simultaneously to stimulate both neurogenesis and angiogenesis at neuroangiogenic foci, where neuronal, glial, and endothelial precursors divide in tight clusters (Palmer et al., 2000; Weinstein, 2005). In adult stem cell niches, as in development, this juxtaposition of neurogenesis and angiogenesis is also found (Fuchs et al., 2004; Alvarez-Buylla and Lim, 2004). Studies in adult male canaries, which undergo a seasonal hypertrophy in the periventricular higher vocal center (HVC) induced by changes in testosterone levels, show both addition of new neurons and endothelial cell divisions in the HVC (Louis-saint et al., 2002). Increases in testosterone levels up-regulate VEGF in neurons and astrocytes; this supports angiogenesis and stimulates the release of brain-derived

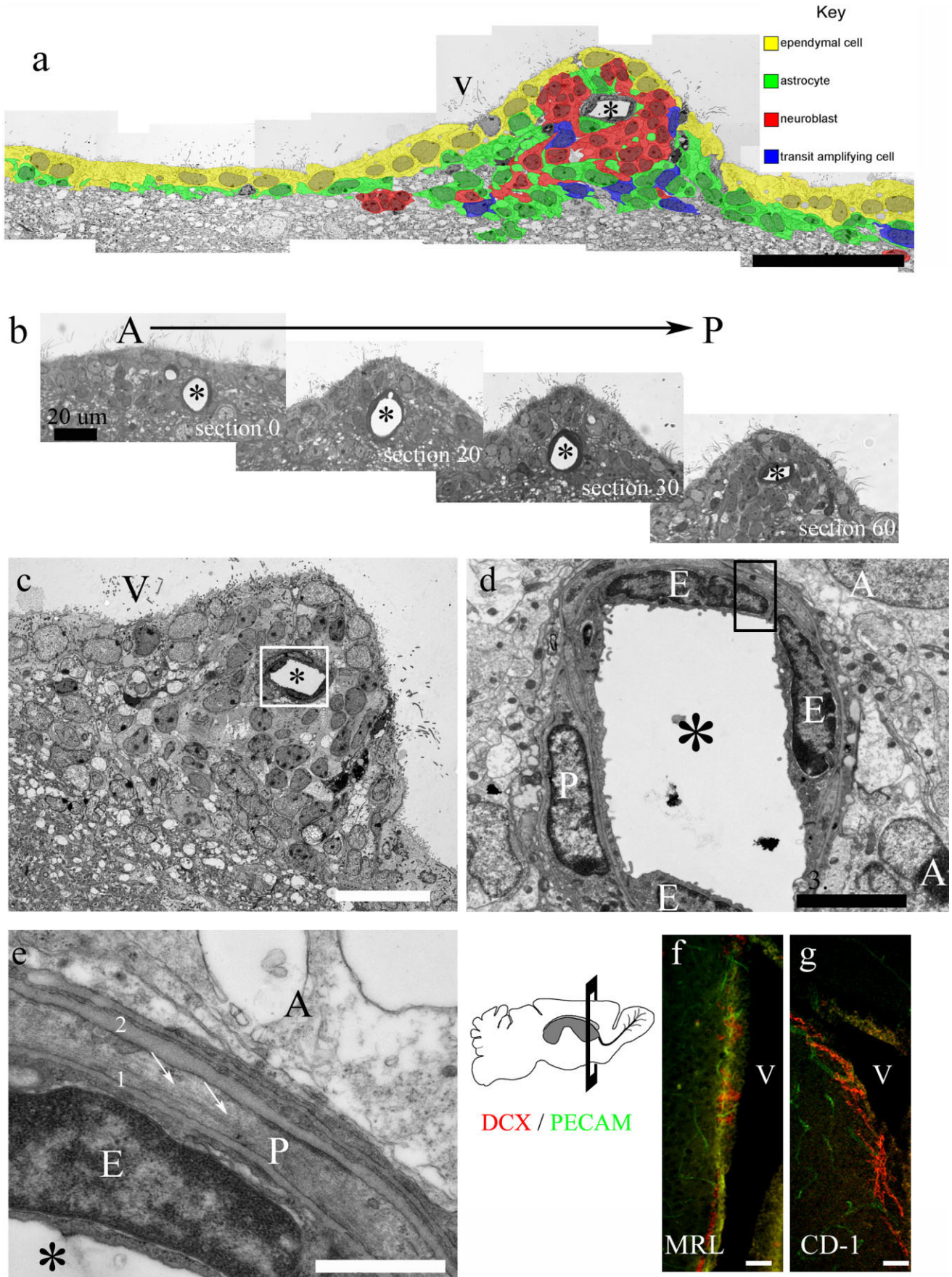


Figure 7

neurotrophic factor (BDNF) from endothelial cells. Increased levels of BDNF then promote migration and recruitment of new neurons in the HVC ventricular zone (Louissaint et al., 2002).

In the MRL mouse, the SVZ also exhibits a close association between blood vessels and areas of neurogenesis. It is possible that SVZ blood vessels help support enhanced neurogenesis (Palmer et al., 2000; Louissaint et al., 2002; Capela and Temple, 2002; Shen et al., 2004); however, perivascular factors may also support the migration of neurons (Kawamura et al., 1988; Wichterle et al., 1999; Louissaint et al., 2002; Weinstein, 2005). As found in birds, it is likely that concordance between angiogenic and neurogenic factors acts to regulate both proliferation and migration within the SVZ. The alterations that we detected in the SVZ of MRL mice may present a variation on neuroangiogenic regulation, allowing support of increased numbers of neuroblasts in this neurogenic zone.

### Enlarged ventricles and increased SVZ proliferation in MRL mice

Enlarged ventricles are typically associated with neurodegeneration and characteristically accompany aging. However, other factors, such as deregulation of stem cell self-renewal, can also contribute to enlarged ventricles. For example, Shi et al. (2004) found that mice lacking TLX, an orphan receptor that maintains NSCs in a proliferative, undifferentiated state, have expanded lateral ventricles. TLX mutant mice have no brain defects during embryogenesis, but they show reduced cell proliferation and few nestin<sup>+</sup> cells in the neurogenic brain regions of the hippocampal dentate gyri and SVZ during adulthood. However, for MRL mice, we detect increased proliferation along the lateral ventricles and aggregates of neuroblasts in subependymal outpocketings. This combination of enlarged ventricles and increased proliferation is more reminiscent of studies by Chenn and Walsh (2002, 2003), in which they observed a greatly expanded proliferative zone, with periventricular heterotopias, adjacent to an enlarged ventricular lumen in transgenic mice expressing a stabilized form of  $\beta$ -catenin in neural precursors. Surprisingly, these transgenic mice not only developed enlarged brains but the increased cerebral cortical surface area was arranged into folds resembling sulci and gyri of higher mammals. The increased proliferation we see in

MRL mice is on a much smaller scale and presents no gross cortical or OB alterations. Our observation that cell death is significantly increased within the OB, but does not increase within either the SVZ or the RMS, suggests that cell numbers and thereby OB size are maintained through regulated cell death. We speculate that the increases in proliferation and the accumulation of neuroblasts found in the SVZ of MRL mice develop from an expanded precursor pool that is maintained throughout development. We hypothesize that the neighboring neurogenic niche of the hippocampal dentate gyrus might also house an enlarged precursor pool to support hippocampal neurogenesis. Similar findings of expanded precursor pools may be observed in other stem cell niches (e.g., hematopoietic, epithelial, and intestinal). However, analysis of enhanced hematopoiesis by means of a wide phenotypic screen of mature hematopoietic components, progenitor populations, and hematopoietic stem cells is confounded by the lack of an appropriate control for the composite genome of the MRL/MpJ mouse strain (unpublished data from Leonardo Aguila, University of Connecticut Health Center).

### Chain migration in the SVZ and RMS of MRL mice

Newly generated neuroblasts migrate as chains along the lateral wall of the lateral ventricle and then travel anteriorly along the RMS into the OB. These chains of neuroblasts are ensheathed by astrocytes. We observed neuroblast chains in whole-mount preparations of the lateral wall of the lateral ventricle in MRL mice. The chains appeared robust and did not show any indications of abnormal formation. In addition, although the RMS diameter was greater in MRL mice, the organization did not appear to be aberrant in any way, and retrovirus-labeled SVZ neuroblasts migrated through the RMS and into the OB. However, we did observe that labeled neuroblasts from the SVZ were still migrating through the RMS up to 4 weeks postlabeling, whereas all labeled SVZ neuroblasts from CD-1 mice had exited the RMS and localized to granule or periglomerular layers at this time point.

Severe migration defects resulting from mutations in the nonmuscle filamin, a protein that cross-links nonmuscle actin, have been identified as a cause for the human disease periventricular heterotopia (Fox et al., 1998), and ablation of nonmuscle myosin II-B heavy chain results in similar periventricular heterotopias (Tullio et al., 2001). In both cases, neural cells fail to migrate to their target destinations and proliferate in periventricular nodules. These migration defects are extreme and differ from what we observe in MRL mice, i.e., normal neuroblast chain formation and the ability for SVZ neuroblasts to migrate into the OB. Instead, our data support the hypothesis that an increased progenitor pool in MRL mice results in more neuroblasts, creating a bottleneck in the anterior SVZ where neuroblasts enter the RMS, thereby slowing migration out of the SVZ. In this model, the formation of neuroblast protuberances is a consequence of increased SVZ proliferation generating increased numbers of neuroblasts. It remains to be determined whether extensive heterotopias develop as MRL mice age or whether SVZ proliferation instead declines with age.

Fig. 7. Association between blood vessels and neuroblastic protuberances. **a:** Colorized montage of assembled EM photomicrographs showing a neuroblastic protuberance containing a capillary. **b:** A series of semithin sections, spanning 60  $\mu$ m anterior to posterior, reveals the close association between the capillary and protuberance shown in **a**. **c:** Slightly more anterior view of **a** reveals cell organization within the protuberance. **d:** Closeup of capillary (boxed area in **c**) shows a pericyte encircling endothelial cells that line the blood vessel. Astrocytes contact the pericyte and endothelial cells. **e:** Higher magnification of boxed area in **d** shows cell-cell interactions. The basal lamina of an endothelial cell (1) contacts the basal lamina of the pericyte (2), which is in contact with a neighboring astrocyte. Note microfilaments within the cytoplasm of the pericyte (arrows). **f,g:** Coronal section of anterior forebrain of MRL and CD-1 mice showing arrangement of blood vessels (PECAM<sup>+</sup>) along the lateral wall of the lateral ventricle and their interaction with doublecortin-positive (DCX) neuroblasts. Asterisk, lumen of blood vessel; V, ventricle; E, endothelial cells; P, pericyte; A, astrocyte. Scale bars = 50  $\mu$ m in **a,f,g**; 20  $\mu$ m in **b,c**; 3  $\mu$ m in **d**; 500 nm in **e**.

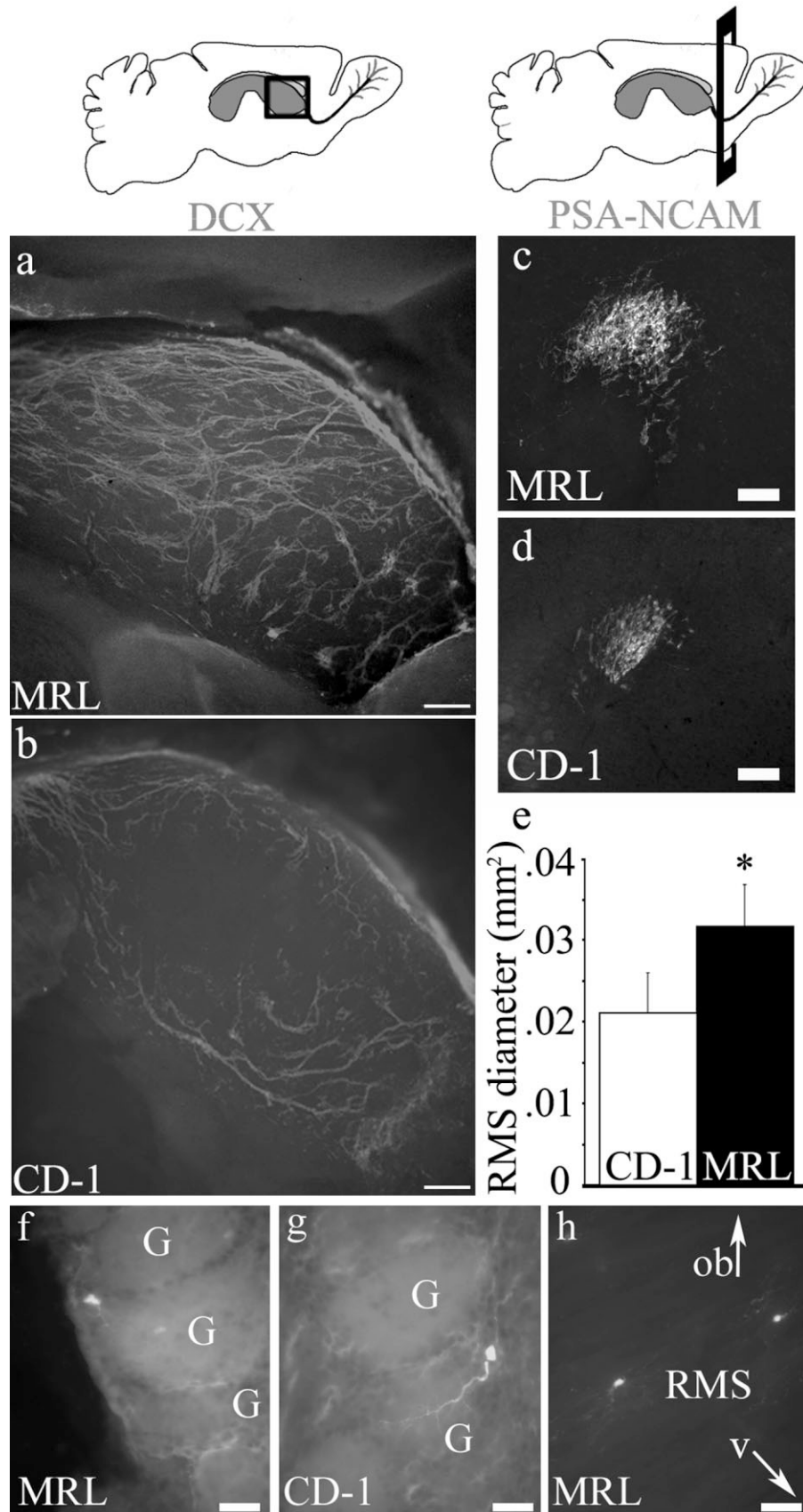


Fig. 8. Neuroblast chain migration in the anterior forebrain of MRL mice. **a,b:** Whole mounts of the lateral wall of the lateral ventricle of MRL and CD-1 mice stained for doublecortin (DCX) show an abundance of neuroblast chains in MRL mice. **c,d:** Representative images of the RMS in MRL compared with CD-1 mice are shown. **e:** Measurements of the RMS diameter, at three different levels, reveal a significant increase in MRL vs. CD-1 mice (*t*-test,  $*P < 0.05$ ). **f,g:**

Tracking eGFP-tagged neuroblasts into the OB reveals that they become incorporated into the granule (not shown) and periglomerular layers 2 weeks postretrovirus injection. G, glomerulus. **h:** However, at 4 weeks postinjection eGFP-tagged neuroblasts are still found migrating through the RMS, while no labeled neuroblasts are found in the RMS of CD-1 mice (not shown). Scale bars = 500  $\mu$ m in a,b; 50  $\mu$ m in c,d; 25  $\mu$ m in f-h.

### The MRL background

The MRL mouse is an inbred mouse with a genetic background of LG (75%), AKR (12.6%), C3H (12.1%), and C57BL/6 (0.3%). In earlier studies, the MRL mouse and the mutant MRL/lpr mouse were developed as congenic strains that differed only in the lpr mutation, a loss of function mutation of the Fas (CD95) gene (Theofilopoulos and Dixon, 1985). The lpr mutation leads to lymphadenopathy and early-onset autoimmune systemic lupus erythematosus (SLE) within 3 months of age, with few mice surviving beyond 6 months of age (Dixon et al., 1978; Ballok et al., 2004). However, it is the inbred background of the MRL mouse that leads to severe lupus, insofar as the Fas-sufficient MRL (MRL/MpJ) strain also develops lupus (late onset at 5–8 months of age, with a survival of up to 2 years). To avoid complications of SLE in our analysis of the neurogenic SVZ, we used 2-month-old MRL mice, which do not show signs of autoimmune disease.

Subependymal neuroblast protuberances were found not only in MRL mice but also in the SVZ of 2-month-old LG mice and the mutant MRL/lpr mice, whereas neither 2-month-old CD-1 nor 2-month-old C57BL/6 mice exhibited these periventricular abnormalities. These results are consistent with the studies of others showing enhanced wound healing in LG mice, but not in most other mouse strains, including CD-1 and C57BL/6 mice (Kench et al., 1999).

The finding that the MRL mouse has heightened wound healing raises the possibility that wound healing and antigen-specific immune responses may be connected (Kench et al., 1999). Particularly noteworthy is the finding that one antibody, detected in the serum of both MRL and MRL/lpr mice, is directed against Ki67, a cell proliferation marker. The presence of anti-Ki67 antibody in MRL mice, but not other autoimmune mice, suggests that it is specific to the SLE that develops in these mice (Bloch et al., 1995). It is tantalizing to speculate that highly proliferative zones that provide the heightened regenerative capacity in these mice might also provide the targets for the autoimmune attack in SLE. However, there are several indications that the wound healing ability in MRL mice is independent of the development of autoimmunity (Kench et al., 1999), and wound healing has been suggested to be a quantitative trait resulting from the contribution of several MRL genes (Clark et al., 1998; McBreaarty et al., 1998).

### CONCLUSIONS

Our findings demonstrate that the MRL mouse strain supports increased proliferation, with the formation of protuberant nests of neuroblasts in the neurogenic niche of the SVZ. It is interesting that this phenotype is similar, but on a much reduced scale, to that found in a model of increased neurogenesis produced through the stabilization of  $\beta$ -catenin (Chenn and Walsh, 2002, 2003). Although it is tantalizing to speculate that the changes we observe in the neurogenic SVZ are part of a comprehensive regenerative program unique to the MRL background, this is still not clear. The naturally occurring loss of OB neurons may represent a requirement for ongoing physiological repair. Whether production of excess neuroblasts in the SVZ actually supports increased incorporation of functional neurons in the OB remains to be determined. Additionally,

because we did not generate a specific brain injury in MRL mice that could potentially activate or utilize the new neurons produced by the SVZ, we do not know whether injury would result in redirection of neuroblasts to the site of insult. Magavi et al. (2000) have shown that progenitor cells, possibly from the SVZ, can be recruited into the adult cerebral cortex following a targeted cortical lesion. Several forms of injury (i.e., cortical aspiration, cortical transection, fimbria fornix lesions, inflammatory demyelination, seizures, stroke, excitotoxic striatal lesions, and fluid percussion injury) increase cell proliferation in the SVZ (Lichtenwalner and Parent, 2006), but it is not clear whether injury-induced neurogenesis results in proper integration and function of newly generated neurons (for recent reviews see Hallbergson et al., 2003; Lichtenwalner and Parent, 2006). Further examination of the MRL mouse, and perhaps its component strain LG, in conjunction with injury models, will provide insights into the mechanisms regulating supply and demand for SVZ neurogenesis. In addition, examination of progenitor pools in other adult MRL stem cell niches will address a possible link between enhanced stem cell niches and regenerative capacity.

### LITERATURE CITED

- Alvarez-Buylla A, Lim DA. 2004. For the long run: maintaining germinal niches in the adult brain. *Neuron* 41:683–686.
- Alvarez-Buylla A, Garcia-Verdugo JM, Tramontin AD. 2001. A unified hypothesis on the lineage of neural stem cells. *Nat Rev Neurosci* 2:287–293.
- Ballok DA, Earls AM, Krasnik C, Hoffman SA, Sakic B. 2004. Autoimmune-induced damage of the midbrain dopaminergic system in lupus-prone mice. *J Neuroimmunol* 152:83–97.
- Belluzzi O, Benedusi M, Ackman J, LoTurco JJ. 2003. Electrophysiological differentiation of new neurons in the olfactory bulb. *J Neurosci* 23:10411–10418.
- Blaschke AJ, Staley K, Chun J. 1996. Widespread programmed cell death in proliferative and postmitotic regions of the fetal cerebral cortex. *Development* 122:1165–1174.
- Blaschke AJ, Weiner JA, Chun J. 1998. Programmed cell death is a universal feature of embryonic and postnatal neuroproliferative regions throughout the central nervous system. *J Comp Neurol* 396:39–50.
- Bloch DB, Rabkina D, Bloch KD. 1995. The cell proliferation-associated protein Ki-67 is a target of autoantibodies in the serum of MRL mice. *Lab Invest* 73:366–371.
- Bouzioukh F, Tell F, Jean A, Rougon G. 2001. NMDA receptor and nitric oxide synthase activation regulate polysialylated neural cell adhesion molecule expression in adult brainstem synapses. *J Neurosci* 21:4721–4730.
- Brunstrom JE, Gray-Swain MR, Osborne PA, Pearlman AL. 1997. Neuronal heterotopias in the developing cerebral cortex produced by neurotrophin-4. *Neuron* 18:505–517.
- Cameron HA, McKay RD. 2001. Adult neurogenesis produces a large pool of new granule cells in the dentate gyrus. *J Comp Neurol* 435:406–417.
- Capela A, Temple S. 2002. *LeX/ssea-1* is expressed by adult mouse CNS stem cells, identifying them as nonependymal. *Neuron* 35:865–875.
- Cecchi GA, Petreanu LT, Alvarez-Buylla A, Mgnasco MO. 2001. Unsupervised learning and adaptation in a model of adult neurogenesis. *J Comput Neurosci* 11:175–182.
- Chenn A, Walsh CA. 2002. Regulation of cerebral cortical size by control of cell cycle exit in neural precursors. *Science* 297:365–369.
- Chenn A, Walsh CA. 2003. Increased neuronal production, enlarged forebrains and cytoarchitectural distortions in beta-catenin overexpressing transgenic mice. *Cereb Cortex* 13:599–606.
- Chojnacki A, Shimazaki T, Gregg C, Weinmaster G, Weiss S. 2003. Glycoprotein 130 signaling regulates Notch1 expression and activation in the self-renewal of mammalian forebrain neural stem cells. *J Neurosci* 23:1730–1741.
- Clark LD, Clark RK, Heber-Katz E. 1998. A new murine model for mam-

- malian wound repair and regeneration. *Clin Immunol Immunopathol* 88:35–45.
- Conover JC, Doetsch F, Garcia-Verdugo JM, Gale NW, Yancopoulos GD, Alvarez-Buylla A. 2000. Disruption of Eph/ephrin signaling affects migration and proliferation in the adult subventricular zone. *Nat Neurosci* 3:1091–1097.
- Cooper O, Isacson O. 2004. Intrastriatal transforming growth factor alpha delivery to a model of Parkinson's disease induces proliferation and migration of endogenous adult neural progenitor cells without differentiation into dopaminergic neurons. *J Neurosci* 24:8924–8931.
- des Portes V, Pinard JM, Billuart P, Vinet MC, Koulakoff A, Carrie A, Gelot A, Dupuis E, Motte J, Berwald-Netter Y, Catala M, Kahn A, Beldjord C, Chelly J. 1998. A novel CNS gene required for neuronal migration and involved in X-linked subcortical laminar heterotopia and lissencephaly syndrome. *Cell* 92:51–61.
- DiSalvo CV, Zhang D, Jacobberger JW. 1995. Regulation of NIH-3T3 cell G1 phase transit by serum during exponential growth. *Cell Prolif* 28:511–524.
- Dixon FJ, Andrews BS, Eisenberg RA, McConahey PJ, Theofilopoulos AN, Wilson CB. 1978. Etiology and pathogenesis of a spontaneous lupus-like syndrome in mice. *Arthritis Rheum* 21(Suppl):S64–S67.
- Doetsch F. 2003. The glial identity of neural stem cells. *Nat Neurosci* 6:1127–1134.
- Doetsch F, Alvarez-Buylla A. 1996. Network of tangential pathways for neuronal migration in adult mammalian brain. *Proc Natl Acad Sci U S A* 93:14895–14900.
- Doetsch F, Garcia-Verdugo JM, Alvarez-Buylla A. 1997. Cellular composition and three-dimensional organization of the subventricular germinal zone in the adult mammalian brain. *J Neurosci* 17:5046–5061.
- Doetsch F, Caille I, Lim DA, Garcia-Verdugo JM, Alvarez-Buylla A. 1999. Subventricular zone astrocytes are neural stem cells in the adult mammalian brain. *Cell* 97:703–716.
- Doetsch F, Petreanu L, Caille I, Garcia-Verdugo JM, Alvarez-Buylla A. 2002. EGF converts transit-amplifying neurogenic precursors in the adult brain into multipotent stem cells. *Neuron* 36:1021–1034.
- Fox JW, Lamperti ED, Eksioglou YZ, Hong SE, Feng Y, Graham DA, Scheffer IE, Dobyns WB, Hirschl BA, Radtke RA, Berkovic SF, Huttenlocher PR, Walsh CA. 1998. Mutations in filamin 1 prevent migration of cerebral cortical neurons in human periventricular heterotopia. *Neuron* 21:1315–1325.
- Fuchs E, Tumber T, Guasch G. 2004. Socializing with the neighbors: stem cells and their niche. *Cell* 116:769–778.
- Gage FH. 2000. Mammalian neural stem cells. *Science* 287:1433–1438.
- Garcia-Verdugo JM, Doetsch F, Wichterle H, Lim DA, Alvarez-Buylla A. 1998. Architecture and cell types of the adult subventricular zone: in search of the stem cells. *J Neurobiol* 36:234–248.
- Gheusi G, Cremer H, McLean H, Chazal G, Vincent JD, Lledo PM. 2000. Importance of newly generated neurons in the adult olfactory bulb for odor discrimination. *Proc Natl Acad Sci U S A* 97:1823–1828.
- Gleeson JG, Allen KM, Fox JW, Lamperti ED, Berkovic S, Scheffer I, Cooper EC, Dobyns WB, Minnerath SR, Ross ME, Walsh CA. 1998. Doublecortin, a brain-specific gene mutated in human X-linked lissencephaly and double cortex syndrome, encodes a putative signaling protein. *Cell* 92:63–72.
- Gleeson JG, Lin PT, Flanagan LA, Walsh CA. 1999. Doublecortin is a microtubule-associated protein and is expressed widely by migrating neurons. *Neuron* 23:257–271.
- Hallbergson AF, Gnatenco C, Peterson DA. 2003. Neurogenesis and brain injury: managing a renewable resource for repair. *J Clin Invest* 112:1128–1133.
- Imura T, Kornblum HI, Sofroniew MV. 2003. The predominant neural stem cell isolated from postnatal and adult forebrain but not early embryonic forebrain expresses GFAP. *J Neurosci* 23:2824–2832.
- Jin K, Peel AL, Mao XO, Xie L, Cottrell BA, Henshall DC, Greenberg DA. 2004. Increased hippocampal neurogenesis in Alzheimer's disease. *Proc Natl Acad Sci U S A* 101:343–347.
- Kawamura K, Nanami T, Kikuchi Y, Kitakami A. 1988. Grafted granule and Purkinje cells can migrate into the mature cerebellum of normal adult rats. *Exp Brain Res* 70:477–484.
- Kempermann G, Wiskott L, Gage FH. 2004. Functional significance of adult neurogenesis. *Curr Opin Neurobiol* 14:186–191.
- Kench JA, Russell DM, Fadok VA, Young SK, Worthen GS, Jones-Carson J, Henson JE, Henson PM, Mazinge D. 1999. Aberrant wound healing and TGF-beta production in the autoimmune-prone MRL/+ mouse. *Clin Immunol* 92:300–310.
- Key G, Becker MH, Baron B, Duchrow M, Schluter C, Flad HD, Gerdes J. 1993. New Ki-67-equivalent murine monoclonal antibodies (MIB 1–3) generated against bacterially expressed parts of the Ki-67 cDNA containing three 62 base pair repetitive elements encoding for the Ki-67 epitope. *Lab Invest* 68:629–636.
- Kuo LT, Simpson A, Schanzer A, Tse J, An SF, Scaravilli F, Groves MJ. 2005. Effects of systemically administered NT-3 on sensory neuron loss and nestin expression following axotomy. *J Comp Neurol* 482:320–332.
- Leferovich JM, Bedelbaeva K, Samulewicz S, Zhang XM, Zwas D, Lankford EB, Heber-Katz E. 2001. Heart regeneration in adult MRL mice. *Proc Natl Acad Sci U S A* 98:9830–9835.
- Lichtenwalner RJ, Parent JM. 2006. Adult neurogenesis and the ischemic forebrain. *J Cereb Blood Flow Metab* 26:1–20.
- Lie DC, Dzieczapolski G, Willhoite AR, Kaspar BK, Shults CW, Gage FH. 2002. The adult substantia nigra contains progenitor cells with neurogenic potential. *J Neurosci* 22:6639–6649.
- Lim DA, Tramontin AD, Trevejo JM, Herrera DG, Garcia-Verdugo JM, Alvarez-Buylla A. 2000. Noggin antagonizes BMP signaling to create a niche for adult neurogenesis. *Neuron* 28:713–726.
- Lois C, Garcia-Verdugo JM, Alvarez-Buylla A. 1996. Chain migration of neuronal precursors. *Science* 271:978–981.
- Louissaint A Jr, Rao S, Leventhal C, Goldman SA. 2002. Coordinated interaction of neurogenesis and angiogenesis in the adult songbird brain. *Neuron* 34:945–960.
- Luskin MB. 1993. Restricted proliferation and migration of postnatally generated neurons derived from the forebrain subventricular zone. *Neuron* 11:173–189.
- Magavi SS, Leavitt BR, Macklis JD. 2000. Induction of neurogenesis in the neocortex of adult mice. *Nature* 405:951–955.
- McBrearty BA, Clark LD, Zhang XM, Blankenhorn EP, Heber-Katz E. 1998. Genetic analysis of a mammalian wound-healing trait. *Proc Natl Acad Sci U S A* 95:11792–11797.
- Mizuguchi M, Qin J, Yamada M, Ikeda K, Takashima S. 1999. High expression of doublecortin and KIAA0369 protein in fetal brain suggests their specific role in neuronal migration. *Am J Pathol* 155:1713–1721.
- Morshead CM, Reynolds BA, Craig CG, McBurney MW, Staines WA, Morassutti D, Weiss S, van der Kooy D. 1994. Neural stem cells in the adult mammalian forebrain: a relatively quiescent subpopulation of subependymal cells. *Neuron* 13:1071–1082.
- Paitel E, Fahrhaeus R, Checler F. 2003. Cellular prion protein sensitizes neurons to apoptotic stimuli through Mdm2-regulated and p53-dependent caspase 3-like activation. *J Biol Chem* 278:10061–10066.
- Palmer TD, Willhoite AR, Gage FH. 2000. Vascular niche for adult hippocampal neurogenesis. *J Comp Neurol* 425:479–494.
- Paxinos GF. 2001. The mouse brain. San Diego: Academic Press.
- Peterson DA. 2002. Stem cells in brain plasticity and repair. *Curr Opin Pharmacol* 2:34–42.
- Petreanu L, Alvarez-Buylla A. 2002. Maturation and death of adult-born olfactory bulb granule neurons: role of olfaction. *J Neurosci* 22:6106–6113.
- Pompeiano M, Blaschke AJ, Flavell RA, Srinivasan A, Chun J. 2000. Decreased apoptosis in proliferative and postmitotic regions of the caspase 3-deficient embryonic central nervous system. *J Comp Neurol* 423:1–12.
- Putz U, Harwell C, Nedivi E. 2005. Soluble CPG15 expressed during early development rescues cortical progenitors from apoptosis. *Nat Neurosci* 8:322–331.
- Quinones-Hinojosa A, Sanai N, Soriano-Navarro M, Gonzalez-Perez O, Mirzadeh Z, Gil-Perotin S, Romero-Rodriguez R, Berger MS, Garcia-Verdugo JM, Alvarez-Buylla A. 2006. Cellular composition and cytoarchitecture of the adult human subventricular zone: a niche of neural stem cells. *J Comp Neurol* 494:415–434.
- Reynolds BA, Weiss S. 1992. Generation of neurons and astrocytes from isolated cells of the adult mammalian central nervous system. *Science* 255:1707–1710.
- Roth KA, Kuan C, Haydar TF, D'Sa-Eipper C, Shindler KS, Zheng TS, Kuida K, Flavell RA, Rakic P. 2000. Epistatic and independent functions of caspase-3 and Bcl-X(L) in developmental programmed cell death. *Proc Natl Acad Sci U S A* 97:466–471.
- Rousselot P, Lois C, Alvarez-Buylla A. 1995. Embryonic (PSA) N-CAM reveals chains of migrating neuroblasts between the lateral ventricle and the olfactory bulb of adult mice. *J Comp Neurol* 351:51–61.
- Sawant LA, Hasegkar NN, Vyasrayani LS. 1994. Developmental expres-

- sion of neurofilament and glial filament proteins in rat cerebellum. *Int J Dev Biol* 38:429–437.
- Scholzen T and Gerdes J. 2000. The Ki-67 protein: from the known and the unknown. *J Cell Physiol* 182(3): 311–22.
- Shen Q, Goderie SK, Jin L, Karanth N, Sun Y, Abramova N, Vincent P, Pumiglia K, Temple S. 2004. Endothelial cells stimulate self-renewal and expand neurogenesis of neural stem cells. *Science* 304: 1338–1340.
- Shi Y, Chichung Lie D, Taupin P, Nakashima K, Ray J, Yu RT, Gage FH, Evans RM. 2004. Expression and function of orphan nuclear receptor TLX in adult neural stem cells. *Nature* 427:78–83.
- Shimazaki T, Shingo T, Weiss S. 2001. The ciliary neurotrophic factor/leukemia inhibitory factor/gp130 receptor complex operates in the maintenance of mammalian forebrain neural stem cells. *J Neurosci* 21:7642–7653.
- Theofilopoulos AN, Dixon FJ. 1985. Murine models of systemic lupus erythematosus. *Adv Immunol* 37:269–390.
- Thomaidou D, Mione MC, Cavanagh JF, Parnavelas JG. 1997. Apoptosis and its relation to the cell cycle in the developing cerebral cortex. *J Neurosci* 17:1075–1085.
- Toma JG, Akhavan M, Fernandes KJ, Barnabe-Heider F, Sadikot A, Kaplan DR, Miller FD. 2001. Isolation of multipotent adult stem cells from the dermis of mammalian skin. *Nat Cell Biol* 3:778–784.
- Tullio AN, Bridgman PC, Tresser NJ, Chan CC, Conti MA, Adelstein RS, Hara Y. 2001. Structural abnormalities develop in the brain after ablation of the gene encoding nonmuscle myosin II-B heavy chain. *J Comp Neurol* 433:62–74.
- van Praag H, Shubert T, Zhao C, Gage FH. 2005. Exercise enhances learning and hippocampal neurogenesis in aged mice. *J Neurosci* 25: 8680–8685.
- Weinstein BM. 2005. Vessels and nerves: marching to the same tune. *Cell* 120:299–302.
- Wichterle H, Garcia-Verdugo JM, Herrera DG, Alvarez-Buylla A. 1999. Young neurons from medial ganglionic eminence disperse in adult and embryonic brain. *Nat Neurosci* 2:461–466.
- Wurmser AE, Palmer TD, Gage FH. 2004. Neuroscience. Cellular interactions in the stem cell niche. *Science* 304:1253–1255.